Editors' Suggestion

Toward a diffraction limited light source

Pantaleo Raimondi and Simone Maria Liuzzo
ESRF, Grenoble, France

(Received 17 October 2022; accepted 17 January 2023; published 22 February 2023)

This paper introduces a storage ring lattice design for synchrotron radiation sources which fulfills all the required features for the realization of a diffraction limited light source. Insertion devices half gaps of 2.5 mm are assumed and enabled by the design of dedicated straight sections. The use of long straight sections is possible for such a lattice and led to the definition of a set of transparency conditions used to minimize the effect of such insertions for on- and off- energy beam dynamics. The design proposed enables an extremely long Touschek lifetime and beam accumulation. A real case study will be shown for large circumference storage ring upgrade lattices.

DOI: 10.1103/PhysRevAccelBeams.26.021601

I. INTRODUCTION

The double bend achromat (DBA) [1] has been the most successful and widespread lattice used for third generation synchrotron-based light sources. It has been (and still is) fundamental for the realization and exploitation of high brightness x rays. Following the DBA success, multibend achromat (MBA) lattices have been designed [2] to reduce the horizontal natural emittance by a factor larger than 30 with respect to DBA, establishing a fourth generation of storage ring (SR) light sources with orders of magnitude increase in brightness and transverse coherence [3]. A few MBA rings have been built (MAX IV [4], SIRIUS [5], Extremely Brilliant Source (EBS) [3,6,7]), and many others are in design or construction worldwide.

A peculiar case of the MBA lattice is the H7BA (Hybrid seven Bend Achromat, for a generic number of dipoles HMBA), developed for the EBS. This lattice has proven to be very effective in addressing the nonlinear dynamics challenges associated with the MBA lattice.

To reach the diffraction limit ($\epsilon_{h,v} < 10$ pm rad for x-ray wavelengths of $\lambda = 1$ Å), the horizontal emittance must be further decreased by at least another factor 10 with respect to current MBA projects/designs. Designing a lattice that delivers such emittance while simultaneously preserving the other many features of the DBA is extremely challenging. HMBA can produce such performances by taking advantage of the flexibility of a green-field project and of the horizontal natural emittance (ϵ_h) scaling law of a large-size facility

$$\epsilon_h \propto \frac{E^2}{N_{\mathrm{bend}}^3}$$

with E the energy of the e^- beam and N_{bend} an integer number of dipoles per cell [2].

The performances of a few of the present and future light sources are displayed in Fig. 1 [7–36]. For most of the existing SR light sources with natural horizontal emittance above $\epsilon_h = 1$ nmrad, the dynamic aperture (DA) is large and energy acceptance (EA) as well. Most of the current upgrades aim to shift the balance in favor of ϵ_h. Projects with a design DA lower than 5 mm become critical for operations with beam accumulation.

This paper will propose a lattice design that could overcome the trend and provide large DA and EA for horizontal emittances below 10 pm rad.

A. Diffraction limited source challenges

According to the authors, the ideal parameters of a diffraction limited light source (DLS) are as follows:

(i) round beam with emittance in both planes of the order of 5–15 pm rad (for x-ray wavelengths of 1 Å),

(ii) e^- beam optics matched to the x-ray beam: $\beta_h^{e^-} = \beta_v^{e^-} = \beta^\gamma = L/2$, where L is the insertion devices (ID) length and $\beta^{e^-,\gamma}$ are the Twiss parameters describing the phase space of the electrons and photons, respectively (this item is mandatory at the diffraction limit [37–39]),

(iii) Touschek lifetime (TL) [40] in excess of 10 h (vacuum lifetime is assumed to be above 100 h),

(iv) transverse dynamic aperture at the injection septum in excess of 10 mm for off-axis injection and beam accumulation,

(v) injection consistent with in-vacuum undulators half-gaps closed to 2.5 mm in both planes [39].

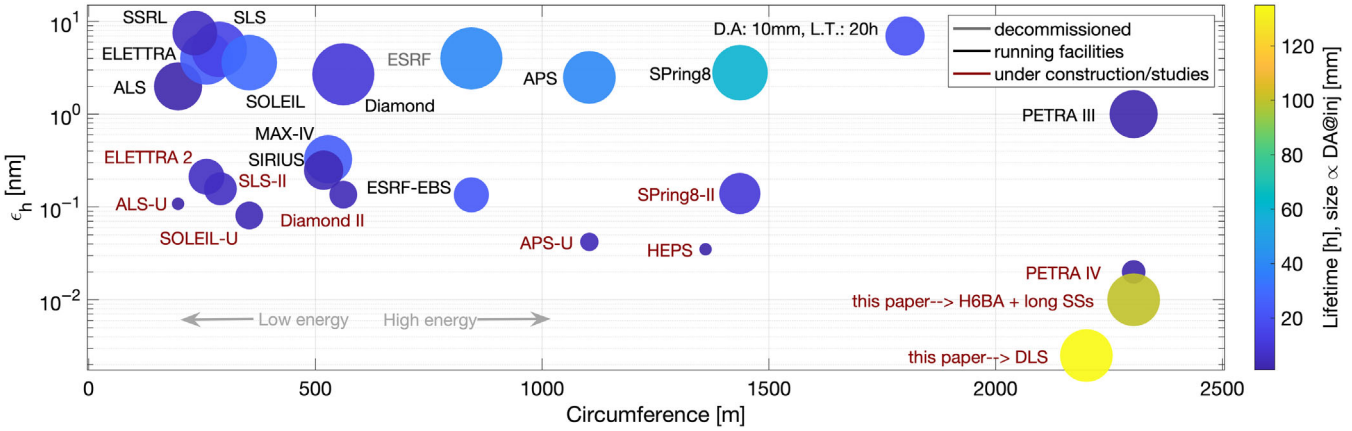

FIG. 1. Dynamic aperture and Touschek lifetime for some of the past, present, and future SR light sources. The size of the circles is representative of the DA and the color is proportional to TL. The data sources for this figure are found in [7–36].

These parameters allow user operations that are very similar to what is currently achieved in all facilities. In addition, they are consistent with the following features:

(i) relaxed injection complex requirements (similar injection concepts as those used for present facilities)

(ii) e^- beam stability during injection and beam decay

(iii) different operation modes: timing modes with few high current bunches, hybrid modes with a long train of low charge bunches and one or few high charge bunches, uniform filling of all bunches, etc. (see [6] for example)

(iv) comfortable radiation handling, in particular, making use of collimators [41]

(v) reduced component activation and ID radiation damage [42]

(vi) reduced operation costs and wall plug power.

A possible path to a factor 10 reduction in horizontal natural emittance compared to MBA lattices ($\epsilon_{h,v} < 10$ pmrad) could be made of four steps. The first step would be to develop an HMBA (with M and the most suitable number of dipoles) that has an equilibrium emittance 3 times smaller with respect to the EBS H7BA: the SR lattice should produce a natural emittance around 30–50 pm. The second step would be to define a layout consistent with the implementation of wigglers to reduce the emittance by another factor 2. This is very convenient since HMBA has a very reduced energy loss due to synchrotron radiation with respect to DBA (and MBA). For example, the EBS H7BA has about half the energy loss of a DBA lattice of the same circumference and energy but no available space for wigglers (see Table I). The third step would be to couple the horizontal and vertical planes in order to reduce the horizontal emittance by another factor $\simeq 2$ ($\epsilon_{h=v} = J_h/(J_h + J_v)\epsilon_h$, where $J_{h,v}$ are the horizontal and vertical damping partition numbers). The vertical emittance will be equal to the horizontal [43]. This is possible only when the horizontal emittance is just about a factor of 2 larger than the desired vertical emittance (the diffraction limited one or the one requested by the user, typically $\epsilon_v = 5$–15 pm). Finally, the last step would be to add long straight sections (SSs) for optimal injection and other purposes. This must be done by limiting as much as possible the drawbacks due to the reduced periodicity of the lattice. A dedicated section of this paper will present a list of *transparency conditions* that enables the inclusion of an arbitrary number of straight sections preserving at most DA and EA.

TABLE I. Parameters of SR lattice sources scaled to 6 GeV, 844 m, and 32 cells.

	DBA	MBA	H7BA
Year	1994	2015	2019
ϵ_h pm rad	3985	321	133
Q_h	36.44	67.20	76.21
Q_v	13.39	26.28	27.34
Natural ξ_h	−130	−80	−99
Natural ξ_v	−58	−80	−82
δ_E%	0.106	0.120	0.094
σ_z mm	3.43	3.18	2.9
J_x	1.00	1.86	1.51
U_0/turn MeV/turn	4.75	3.64	2.61
No. of magnets/cell	19	41[4]	32

II. THE EVOLUTION OF MULTIBEND SR LIGHT SOURCE LATTICE

We will introduce in this paper a storage ring lattice design for SR light sources that fulfills all the above-stated features, thus enabling the realization of a DLS. For the sake of clarity, we start with a chronological summary of the choices made for existing SR light sources.

A. DBA lattice

Many third generation SR sources are based on double-bend achromat lattice, with a local dispersion bump for chromaticity correction in the center of the cell (see Fig. 2).

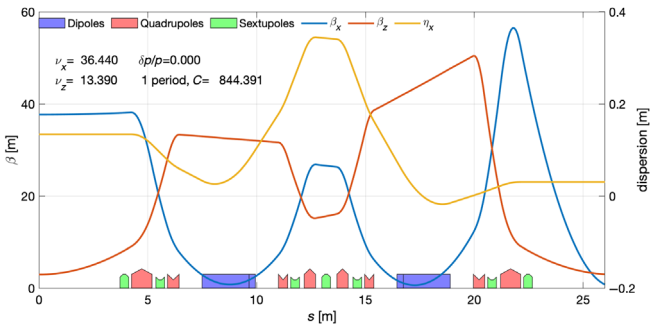

FIG. 2. Optics functions and magnet layout for a DBA lattice cell.

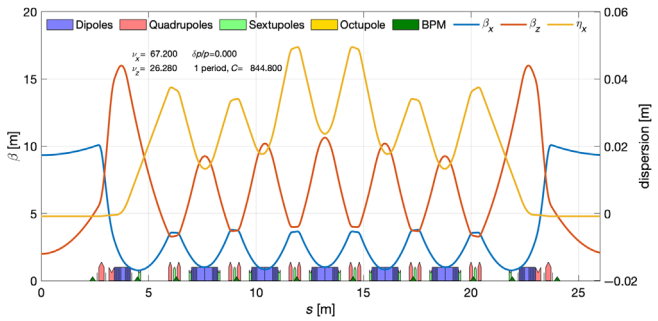

FIG. 3. Optics functions and magnet layout for a 7BA lattice cell.

The dispersion was originally matched to zero in the ID straight sections. Later, the condition was released to reduce the natural horizontal emittance with a better matching of beta function and dispersion at the dipoles and thus reduced $\mathcal{H} = \beta\eta'^2 + 2\alpha\eta\eta' + \gamma\eta^2$ (with β, α, and γ, the Twiss parameters and η, η', the dispersion and its derivative along the beam trajectory).

The Chasman-Green's DBA lattice is not the best solution for horizontal emittance but makes the rescalability of the design very large, preserving sufficient DA and EA for SR light source operation. This is why it has been widely adopted all around the world.

On the contrary, the range of scalability of very specialized and optimized solutions can be very small.

Chasman and Green found an extremely elegant solution to match the optimal phase advance for the DBA [1]: the ID β_h are heavily mismatched and optimized to achieve the best phase advance in terms of overall DA and EA performances.

For ultralow emittances, such a degree of freedom is no longer usable. Maximum performances are achieved when the e^- beam and x-ray phase space at the source are equal. This translates in equal Twiss parameters ($\beta^{e^-} \simeq \beta^{\gamma}$) at the source. The best value for β^{γ} is approximately half the undulator length [39]. Finally, assuming undulators filling whole straight sections, this fixes $\beta^{e^-}_{h,v} = \beta^{\gamma} \sim 2$–$3$ m at the center of the ID SSs.

The undulators placed in the low-beta sections of a DBA (see Fig. 2 at $s \sim 25$ m) produce a heavily depressed x-ray spectrum. For the EBS SR that replaced the DBA lattice with an HMBA lattice, the beamlines that used to operate in the straight sections with low $\beta^{e^-}_h$ have gained about a factor of 30 in flux, thanks to a better matched horizontal $\beta^{e^-}_h$ (~7 m instead of 0.36 m), not because of the smaller ϵ_h.

B. MBA lattice

In order to get small ϵ_h, dipoles have to be many and weak. As a consequence, sextupoles become very strong, take space, and heavily affect the DA and EA properties of the machine.

The MBA lattice [2,4,25] (see Fig. 3) enforces this principle and is successfully used for MAX IV and other storage ring upgrade projects.

No dispersion bump is present in the cell. The number of dipoles used in the lattice cell is a trade-off between lower horizontal natural emittance and sextupole strengths.

Octupoles are introduced in the lattice optics to control transverse amplitude dependent detuning and thus obtain optimal DA.

C. HMBA lattice

The HMBA lattice deals with the problem of efficient chromaticity correction by mirroring two chromaticity correction sections (CCS) similar to the DBA cell and building an optic in between them that cancels the second order (and most of the third) nonlinearities introduced by the strong sextupoles [44]. The Hybrid Seven Bend Achromat (H7BA) cell of EBS is shown in Fig. 4.

The H7BA unifies the advantages of the DBA and MBA cells including multiple bends for lower natural horizontal emittance as in the MBA cell and two dispersion bumps as those of the DBA cell paired by a $-\mathcal{I}$ transformation for efficient chromaticity correction. This arrangement allows for fewer sextupoles than in a DBA cell (6 instead of 7) with fields <0.6 kT/m. The longer and weaker dipoles lead to less synchrotron radiation. Thus, there is no need of "large" dispersion on the inner dipoles hence small $\mathcal{H}$, ϵ_h and intrabeam scattering are achieved.

Table I lists a few parameters of the three lattice solutions recalled above scaling to the same e^- beam energy (6 GeV), storage ring circumference (844 m) and number of cells (32 cells).

III. SCALING OF DYNAMIC APERTURE AND TOUSCHEK LIFETIME AS A FUNCTION OF THE SEXTUPOLE STRENGTHS

The ESRF EBS H7BA lattice cell provides DA ~ 8 mm and TL ~ 30 h [7] for the most frequently used multibunch filling modes ($I_{\text{bunch}} = 0.2$ mA).

However, these two values are directly related to the strengths of the sextupoles. In fact, DA scales inversely

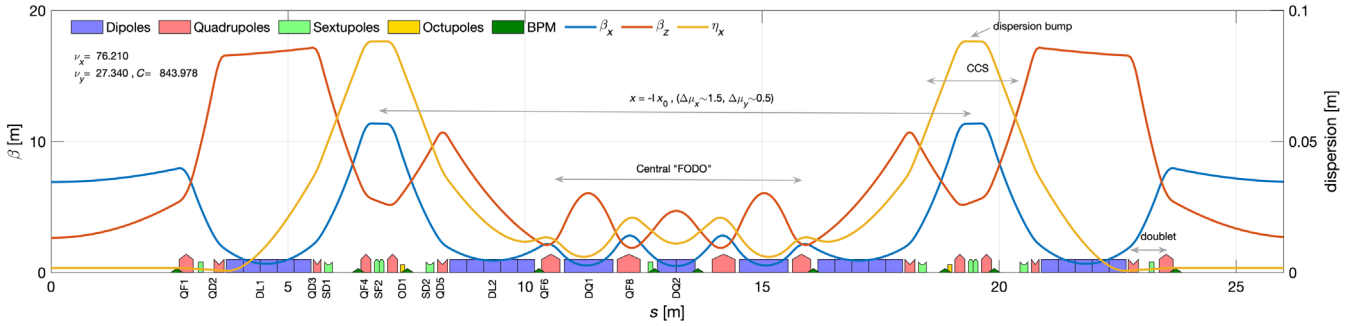

FIG. 4. Optics functions and magnet layout for the EBS H7BA cell.

with the product of sextupole strengths for chromaticity correction

$$\mathrm{DA} \propto \frac{1}{K_{\mathrm{SF}} K_{\mathrm{SD}}}, \tag{1}$$

where $K_{\mathrm{SF,SD}}$ are the gradients of the two families of sextupoles SF and SD used for chromaticity correction. Also, the EA scales similarly, and the TL thus goes down with the third power of the product [40]:

$$\mathrm{TL} \propto \left(\frac{1}{K_{\mathrm{SF}} K_{\mathrm{SD}}}\right)^3, \tag{2}$$

Since the dipoles fields decrease linearly with the number of cells, dispersion decreases linearly and the sextupole strengths increase linearly to correct the natural chromaticity:

$$\xi_{h,v} \propto \sum -K_{\mathrm{quad}} \beta_{h,v}^{\mathrm{quad}} + K_{\mathrm{sext}} \beta_{h,v}^{\mathrm{sext}} \eta_{h,v}^{\mathrm{sext}}.$$

For a machine that is composed of twice the number of cells identical to the ESRF-EBS (64 cells), $K_{\mathrm{sext,64\,cells}} = 2 \times K_{\mathrm{sext,32\,cells}}$ the expected ϵ_h, DA, and TL are as follows:

$$\epsilon_h = (1/2)^3\ 133\ \mathrm{pm} = 16.6\ \mathrm{pm}\ ([2]),$$
$$\mathrm{DA} = [1/(2\times 2)]\ 8\ \ \mathrm{mm} = 2.0\ \mathrm{mm}\ \ \mathrm{Eq.}(1),$$
$$\mathrm{TL} = [1/(2\times 2)]^3\ 30\ \mathrm{h} = 28\ \ \mathrm{min}\ \ \mathrm{Eq.}(2),$$

simply because K_{SF} and K_{SD} are twice as strong. Such scaling was confirmed also in tracking simulations.

Specific conditions can further degrade the performances of a simply scaled lattice cell. For example, a shorter total cell length than the EBS one or the requirement for specific long SSs for injection, special experiments, or simply to fit the existing building infrastructure. In fact, long SSs are particularly detrimental as they break the symmetry of the lattice and need special care in their design. This will be discussed later in detail showing how to actually reduce their impact to the theoretical minimum possible.

The EBS H7BA lattice cell used for a source twice as large leads to a machine that operates very differently with respect to presently operational SR light sources, requiring a more complex injection scheme (such as swap-out [45,46]) and producing high radiation levels due to the reduced lifetime, potentially affecting operation, safety, and lifespan of the components.

IV. A NEW CELL FOR DLS: CELL-U

The design of an SR lattice cell fulfilling all the requirements listed in the introduction of this document is analyzed here starting from the boundary conditions and the budget available for a typical cell (in fact half of the cell, since the other half is mirrored). The conditions assumed to design half SR lattice cell are as follows: 13.1 m available length and 44 mrad total bending angle, corresponding to a ring of 1.9 km circumference and 72 identical cells. The following is a minimum list of needs defined as a sequence starting from the hypothetical undulator center:

(i) 2.5 m are needed for the undulator,

(ii) $\beta^{e^-} = L/2 = 2.5$ m since the e^- and x-ray beams phase space must be matched for best ID performances,

(iii) 1.0 m is needed for a quadrupole triplet QD-QF-QD in order to refocus the divergent beam,

(iv) a minimum of about 30 mrad dipole and 2.0 m is needed to provide the separation between the e^- beam and the x rays,

(v) about 30 mrad dipole and 2.0 m (that may be the same as the previous point) are needed to create enough dispersion for sextupoles with as small as possible gradients,

(vi) 2.0 m are needed for a chromatic correction section,

(vii) 14-mrad dipole and 2.0 m are needed to get to 44-mrad total bending angle.

Only 2–3 m of the 13.1 m available are left for all remaining needs: additional quadrupoles, flanges, bellows, bpms, etc…

The listed sequence of elements naturally produces an overall phase advance of the cell very close (almost exact in fact) to $n\pi$ in both planes. This is an additional nontrivial problem to be solved.

The cell described above is named in this document CELL-U and should be imagined as one of the several identical cells composing an ARC-U. This cell is meant to host undulators filling the whole straight section and must be conceived considering the specificity of a given SR source. Several existing SRs are composed only of such cells.

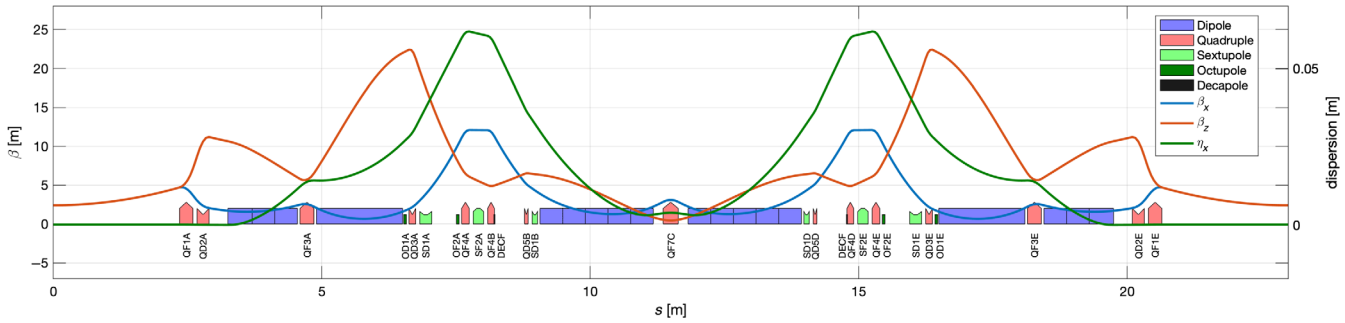

FIG. 5. Optics functions and magnet layout for an H6BA lattice cell designed for a 6 GeV, 72 cells SR lattice.

A. H6BA CELL-U

A solution for a green field project ring fitting almost all the requirements to design CELL-U could be the EBS H7BA cell.

The most difficult to achieve requirements are matched optics at the ID. The H7BA has little control over the ID betas, they can only be modified by a large change in the overall cell phase advance. Also, a compromise has to be found to limit the impact on ϵ_h, DA, and EA.

With respect to the H7BA, at least one additional quadrupole is needed to have enough degrees of freedom to control the betas more effectively. The two quadrupole doublets adjacent to the straight sections (see Fig. 4) should become triplets. To produce a lattice with matched optics at the IDs, the first dipole of the H7BA has been cut into two parts and a QF (focusing quadrupole) has been inserted in the middle. This allows the freedom to choose the ideal phase advance in both planes for the cell while matching the optics at the ID. The additional quadrupole has been added in an optimized position in the middle of the first dipole. Figure 5 shows the new layout of the dipoles for s less than 10 m.

In addition, this choice lowers the final $\mathcal{H} = \beta\eta'^2 + 2\alpha\eta\eta' + \gamma\eta^2$ built by the dipole (see Fig. 4) and matches the natural $\mathcal{H}$ of the second (weaker) dipole.

Most of the H7BA cell dipoles are permanent magnets with longitudinally varying fields [47,48]. An additional quadrupole field is included in these permanent magnets. This moderate gradient in the dipoles led to improved matching of the optics and reduced vertical natural chromaticity. The gradient is set such that the pole face profiles of all dipoles are identical and thus scale with the field in the specific dipole module.

Eventually, the cell horizontal phase advance increases by 0.5 with respect to H7BA, but the horizontal chromaticity increases only by about 10%.

As already mentioned, for very specialized lattices such as MBA and HMBA, the scalability of the cell design to different dimensions is not immediate in view of the scalings in Eqs. (1) and (2). A more effective approach is to tailor the best lattice to a given layout. In particular, the number of dipoles composing a multibend lattice should reduce when increasing the number of cells, to maximize the dispersion generated at the sextupoles. For example, an SR composed of 24 cells could be a nine-bend achromat, one composed of 32 cells, a seven-bend achromat, and one of 64 cells, a six-bend achromat.

It is in fact possible to achieve all the requirements for CELL-U of a DLS source with an H6BA lattice cell (see Fig. 5).

For an H6BA CELL-U, the strong and very chromatic FODO (focusing-drift-defocusing-drift, see [44]) lattice composed of combined function dipole quadrupoles and high gradient focusing quadrupoles [44] present in the EBS H7BA lattice between the sextupoles CCS is removed. A single quadrupole replaces the FODO in the middle of the cell and ensures the "$(-\mathcal{I}_h, -\mathcal{I}_v)$" cancelation between the sextupoles in both planes [44] ($(-3\mathcal{I}_h, -\mathcal{I}_v)$ for EBS). This central quadrupole may also be a quadrupole triplet (see Fig. 5) and is in any case composed of short and weak quadrupoles.

The removal of the FODO lattice in the center of the cell (see Fig. 4) and the withdrawal of the extraction channel for the production of x rays from short bending magnets [7] in the cell center are the main differences with respect to the EBS H7BA.

This H6BA CELL-U has striking DA and EA properties, as visualized later in Sec. V E.

Table II summarizes the main parameters for a ring composed of 72 CELL-U.

The position of all the magnets (dipoles, quadrupoles, sextupoles, octupoles, and a decapole) in the H6BA CELL-U has been optimized to achieve the lower possible strengths and simultaneously to be as effective as possible to minimize the tune variation with transverse amplitude and with momentum. For example, the defocusing octupoles (OD in Fig. 5) are placed at a location of high vertical beta and among all available, the one with the most effect on the control of vertical tune variation with vertical amplitude has been selected.

1. Optics matching for H6BA

Cell-U shares most optics matching knobs with the EBS H7BA lattice. These knobs are represented by the optics

TABLE II. Main parameters of a ring composed of 72 CELL-U.

Parameter	value (Horizontal, Vertical)
ϵ_h	38.4 pm
ϵ_h closed gaps	20.1 pm
U_0	1.151 MeV/turn
U_0 closed gaps	3.097 MeV/turn
Cell length	23.00 m
Cell total phase advance	(1.753, 0.906)
Natural chromaticity	(−179, −208)
Damping partition	(1.78, 1.0, 1.22)
Dipole filling ratio[a]	48.27%
max $\lvert K_{\mathrm{quad}}\rvert$	110 T/m
max $\lvert K_{\mathrm{sext}}\rvert$	1965 T/m^2
max $\lvert K_{\mathrm{oct}}\rvert$	40361 T/m^3

[a]Straight sections excluded.

values at defined locations and are selected to uniquely determine the magnet strengths. These knobs are key ingredients to be able to optimize the optics and to reproduce the desired features when including additional constraints or information at an advanced state of the lattice design. The necessary optics knobs are as follows: $\beta_{x,y}$ and η_x at the ID for undulator optics matching, β_x at the QF4A, η_x at the cell center, α_y at the QD2A, the total phase advance $\mu_{x,y}$, and total chromaticity of the lattice. Further knobs are included to have an almost orthogonal impact on relevant observables. In particular,

(i) the horizontal phase advance between focusing sextupoles $\Delta\phi_x^{\mathrm{SF-SF}}$ is used to control the horizontal detuning with amplitude $(\Delta Q_h/\Delta h)$,

(ii) the vertical phase advance between focusing sextupoles $\Delta\phi_y^{\mathrm{SF-SF}}$ and α_y at the SF are used to control the variation of tunes when moving on the opposite plane $(\Delta Q_h/\Delta v,\ \Delta Q_v/\Delta h)$,

(iii) an octupole OD placed close to the SD is used to control the vertical detuning with amplitude $(\Delta Q_v/\Delta v)$,

(iv) the unbalance of SD sextupoles before and after the SF sextupoles (at fixed chromaticity) is used to control the variation of tunes when moving in a direction defined by $x = y$ $(\Delta Q_{h,v}/\Delta h = v)$,

(v) a decapole is used to control second order chromaticity.

An iterative process led to the definition of the optimal knobs values to get small ϵ_h and large DA and EA for Cell-U. Any modification to the cell requires a revision of these optimal values. As for the EBS H7BA, a small horizontal dispersion in the SS helps to reduce the invariant $\mathcal{H}$ in the cell. The value chosen for the dispersion in the SS is the one that corresponds to the maximum brightness.

V. LARGE RINGS

For large rings (with a circumference of more than 1.2 km), it is not easy to design a lattice that preserves good DA and EA as the two follow the scaling laws shown in Eqs. (1) and (2). In large low emittance rings in fact, dipoles become weak and consequently sextupoles are strong.

The PETRA [36,49] and PEP [50,51] upgrades have all synergies with what could be done on an existing large circumference ring.

In 2021, work was carried out on possible solutions applicable to such large rings, targeting $\epsilon_h < 10$ pm.

In both cases, the structure is modular. It is composed of 72 cells divided into sectors by six or eight straight sections as shown schematically in Fig. 6. This modular structure may be used to separate the ring into dedicated purpose sections.

The components used to transform such large storage rings in DLS are then reassessed as follows, fitting the existing layout:

ARC-U: (U for Undulators) is composed of several CELL-Us and optimized for the best delivery of the target beam to the users with optimal DA and EA. The design should be consistent with the best engineering and hardware performances.

ARC-D: (D for Damping) is composed of several CELL-D and optimized for optimal DA/EA and minimum equilibrium emittance

1 SS: could provide the final damping needed in order to reach the target emittance and emittance leveling

1 Injection SS: provide the optimal injection conditions

1 rf SS: accommodates all the necessary rf

Other SS: with optimized optics adapted to the layout.

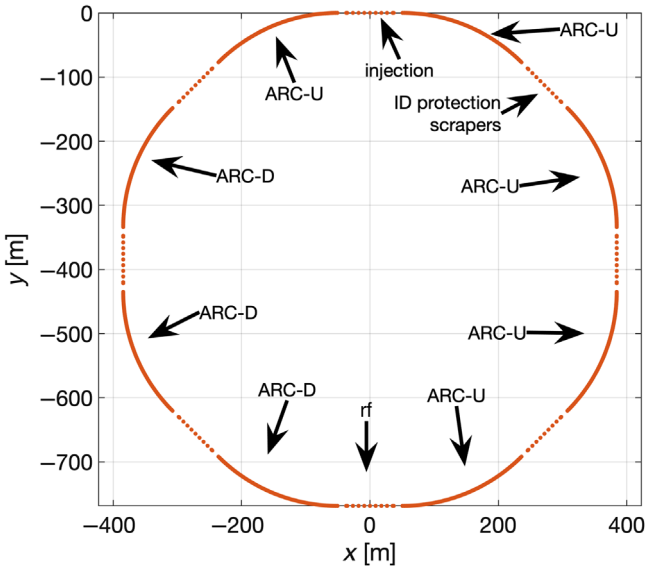

FIG. 6. Footprint of an SR similar to PETRA composed of 72 cells divided in eight ARCs, four long straight sections, and four short straight sections. One of the short straight sections is dedicated to rf and one to injection.

The ARC-Us are composed of several CELL-Us based on the H6BA cell described above. Cell-D and the SSs are addressed in the following sections.

A. Cell-D design: H6BA

CELL-D (one of those composing ARC-D) must bring the emittance down for the ring as a whole and preserve the DA/EA provided by the CELL-U arcs.

Looking at the expected foreseen undulator portfolio of ultralow emittance light sources, it is clear that at full capacity, CELL-U plus the undulators delivers already the target emittance. This is especially true because of the very small H6BA energy loss U_0 (1.15 MeV/turn), thanks to the 48% dipoles filling ratio. In fact, there is hardly anything better in terms of emittance, DA, and damping with respect to the combination of CELL-U+undulators (see Fig. 7 and Table IV).

The simplest and most effective solution is then to make CELL-D equal to CELL-U with wigglers (0.56 T, 10-cm period) installed in the available straight sections of the cells in ARC-D. This solution freezes all the machine parameters, independently of the ID gap settings defined by the users of x rays emitted from ARC-U sectors. A feedback keeps ϵ_h constant by acting on the wigglers gaps in CELL-Ds. All other parameters will be consequently constant as well: lifetime, U_0, bunch length, etc… It is conceivable that the wigglers in *user service mode* will on average produce a damping of about 30% of the total (down to 0% with all IDs at their minimum gap). The wigglers will operate at full power just during *machine dedicated time* and even then, only if needed.

B. Introduction of specific purpose straight sections

Specific purpose straight sections have to be designed to fit the existing tunnel geometry in upgrade projects and/or to provide specific optics for the operation of the SR source. As an example, we discuss here the introduction of a straight section dedicated to injection in the storage ring. For the EBS lattice, a dedicated injection cell [52] increases the horizontal beta functions at the injection point to reach above 90% injection efficiency (given the injectors configuration [7]).

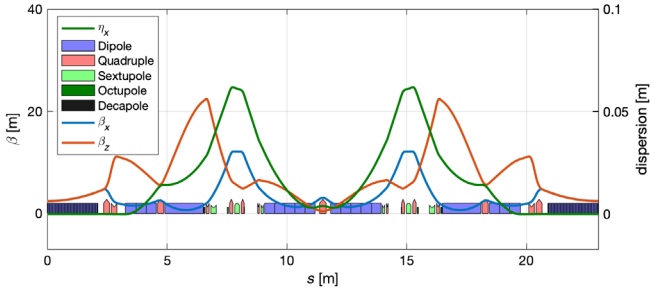

FIG. 7. H6BA CELL-D lattice cell.

Also for a DLS, a dedicated injection straight section has to be optimized to reach a DA consistent with electron beam accumulation and to be able to inject in the SR with small aperture IDs gaps in both planes (as it will be described later in Sec. VI).

1. Transparency conditions for the introduction of arbitrary straight sections

If no action is taken, the introduction of such insertion in the lattice strongly reduces the overall performance [53].

The problem of limiting the degradation of the DA and EA of the full system including CELL-U and specific straight sections such as the injection one is not trivial.

$\xi_{h,v}$ being the chromaticity of the ARCs only, the straight sections (see, for example, Figs. 8 and 9) add unavoidable chromaticity $\Delta\xi_h$ and $\Delta\xi_v$ therefore, the ARC sextupoles become stronger:

$$\Delta K_{\mathrm{SF}}/K_{\mathrm{SF}} = \Delta\xi_h/\xi_h \tag{3}$$

$$\Delta K_{\mathrm{SD}}/K_{\mathrm{SD}} = \Delta\xi_v/\xi_v. \tag{4}$$

The minimum degradation for the DA and EA then follows the scaling law described by (1) and (2).

The following *transparency conditions* allow to limit the reduction to the minimum defined by the increased natural chromaticity.

In the middle of the cell shown in Figs. 8 and 9, supposing the arc is a single pass transfer line, the optics must satisfy these constraints:

I. to ensure the periodicity for on-energy electrons:

(i) The additional horizontal cell phase advance introduced by the SS must be $\Delta\mu_h = 0 + N$, with N an integer [53].

(ii) The additional vertical cell phase advance introduced by the SS must be $\Delta\mu_v = 0 + M/2$, with M an integer.

(iii) The Twiss parameters $\alpha_{h,v} = 0$ and $\eta'_h = 0$.

II. to ensure the periodicity for off-energy electrons in first order:

(i) $\frac{\partial W_{h,v}}{\partial s} = 0$ where $W_{h,v}$ are the Montague functions [54].

(ii) $\frac{\partial \eta'_h}{\partial \delta} = 0$.

III. the overall chromaticity of the CELL-U plus half SSs (e.g., from 0 to 75 m in Fig. 8) should be as close as possible to the one of CELL-U.

IV. for a lattice with superperiodicity P and tune Q, the fractional part of Q/P should be far from 0 and 0.5. The optimal would be for the fractional part of Q/P to be about 0.2–0.3.

All these *transparency conditions* can be achieved by properly selecting the adequate quadrupole locations and adjusting the quadrupole strengths via linear optics matching.

For example, to define the injection cell with large β_h locations of Fig. 9, the optics matching script includes a sufficient number of variables (quadrupoles and their

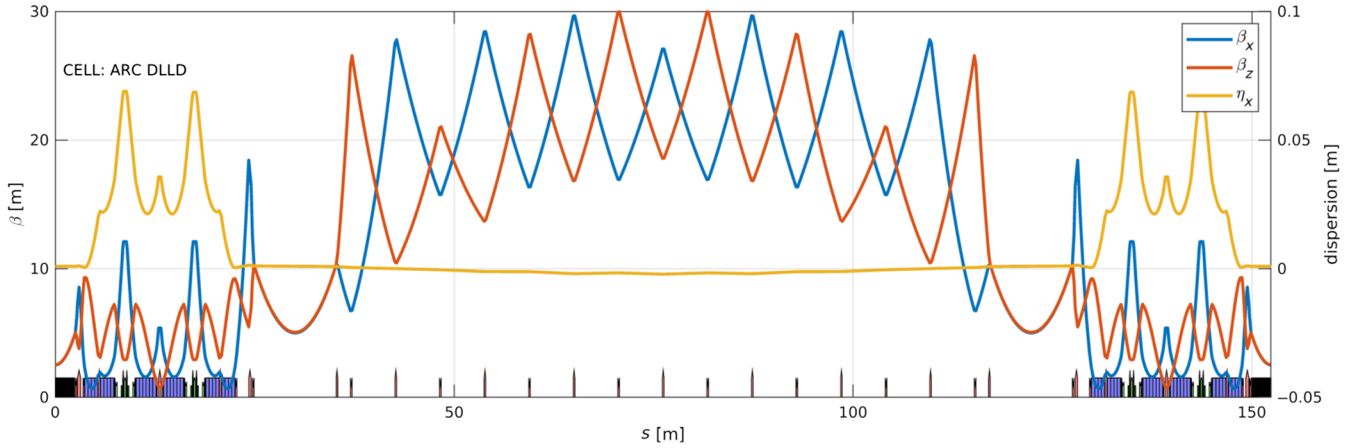

FIG. 8. Example of the long straight section, $L = 103$ m, with two peculiar regions with $\beta_h = \beta_v = 5$ m at $s \sim 30$ and 120 m.

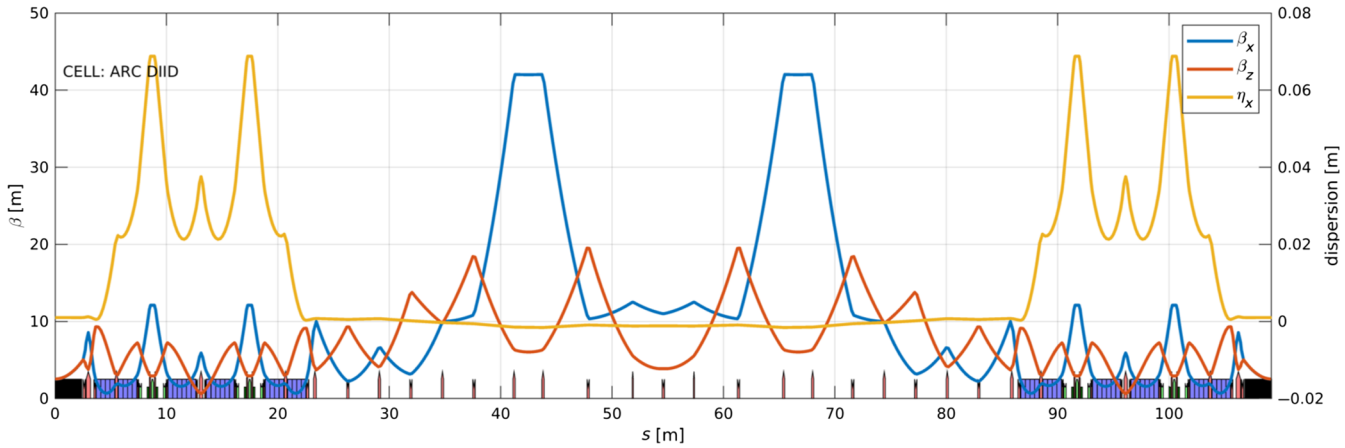

FIG. 9. Injection straight section, beam abort septum at $s = 42$ m, and injection septum at $s = 67$ m with $\beta_h = 42$ m.

locations for example) to set β_h at will and to respect all the on-energy and off-energy transparency conditions. These variables include also the elements of the CELL-U or CELL-D neighboring to the SS as can be seen in Figs. 8 and 9.

To achieve the off-energy transparency condition, the dispersion suppressor dipoles adjacent to the injection straight section may need to be rearranged. Condition II restores the periodicity of the chromatic functions. Notably, they remain periodic with sextupoles powered or with sextupoles set to zero (because of condition I). No additional sextupole families are needed apart from those used for chromaticity correction.

The transparency conditions totally release the symmetry requirements, allowing for complete flexibility (given a closed geometry) in the location and specific optics of long straight sections. Only the total chromaticity introduced by the SS will limit the DA and EA properties of the ring.

As an example, a worst case highly chromatic straight section (the one in Fig. 8) is repeated 8 times in the lattice and separated by ARC-Us and ARC-Ds. The variation of horizontal and vertical tune with amplitudes and with momentum is shown in Figs. 10 and 11 at the center of an ID straight section ($\beta_h = \beta_v = 2.25$ m). Following the transparency conditions detailed above, those curves are almost unchanged by the presence of the additional straight sections.

Although particles when crossing the half integer resonance are still in the DA/MA acceptance, they exercise large oscillations that can lead to an electron beam halo.

2. *Straight section design*

The design of short SSs (56.8 m), long SSs (103 m, see Fig. 8), and an injection SS (see Fig. 9) has been made with the aim of reducing the degradation as close as possible to the minimum theoretically achievable following the transparency conditions described above.

It should be noted that those criteria also make so that two sextupole families in the ring are sufficient (those used

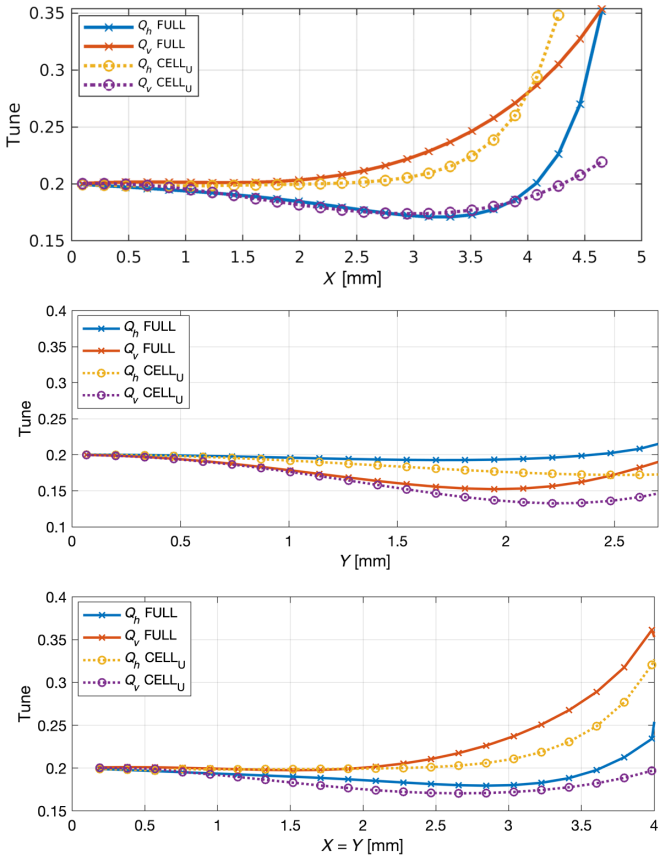

FIG. 10. Variation of tunes with amplitude at the center of an ID straight section ($\beta_h = \beta_v = 2.25$ m) for a lattice composed of only Cell-U ($CELL_U$ in the legend) or including eight SSs ($FULL$ in the legend) following the transparency conditions.

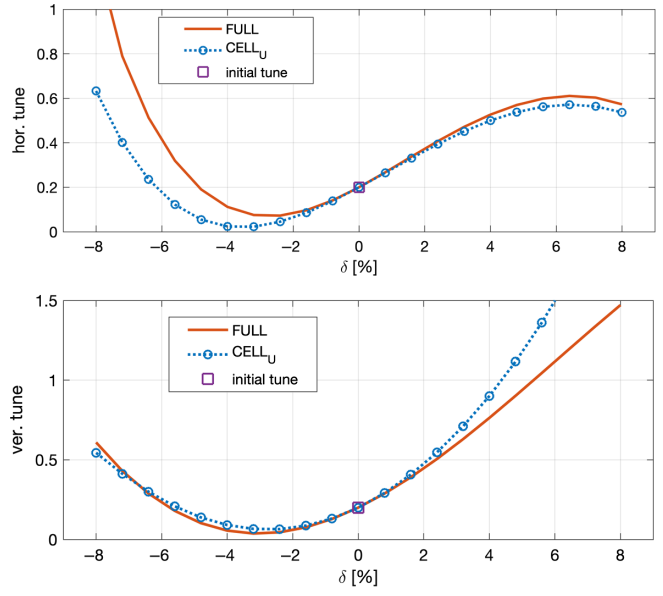

FIG. 11. Variation of tunes with momentum at the center of an ID straight section ($\beta_h = \beta_v = 2.25$ m) for a lattice composed of only Cell-U ($CELL_U$ in the legend) or including eight SSs ($FULL$ in the legend) following the transparency conditions.

for chromaticity correction). More families do help to maximize DA and MA.

The capability of successfully inserting any SSs in a ring is fundamental. A modular design with dedicated sections with optimized functions is a key ingredient for diffraction limited synchrotrons (DLS).

A possible ring layout is then realized by the optics visible in Fig. 12 and includes five ARC-Us, three ARC-Ds, three short (56.8 m) SSs, four long (103 m) SSs, and one injection SS (56.8 m). A more detailed study of a lattice design based on the H6BA cell for the successor of PETRA III, PETRA IV [49], is also being prepared at the time of writing this document.

C. Optimal H6BA working point

The integer part of the tunes for ARC-U and ARC-D has been chosen such that the transparency condition IV is satisfied. For the lattice in Fig. 12, the best tune to be set for the ARC-U and ARC-D sectors would be 127, as $127/72 = 1.764$, far from 1.5 and 2.0. This working point is optimal (large DA and EA) for a ring composed of only CELL-U. Nevertheless, considering the superperiodicity of eight ARCs, then each arc contributes 15.9 units. This is very close to integer and leads to a more difficult matching of the straight sections. An integer tune of 126, not far from the optimal 127 is instead also appropriate considering the eight arcs superperiodicity, such that the fractional parts of $126/72 = 1.75$ and $126/8 = 15.75$ are both far from 0.5 and 1.0.

The working point 126.2 is close to the optimal for a full periodic ring (127.2) but satisfies the superperiodicity condition IV as well, thus relaxing the introduction of straight sections.

H6BA is very versatile and also different vertical tune working points have been explored. The H6BA presented in these pages has been optimized on a low vertical phase advance giving more relaxed optics with fewer and weaker magnets (see Table III), in particular, the ID matching quadrupoles and the octupoles. Table III shows the difference in gradients and lengths of the magnets for two H6BA lattices with different vertical tunes. Also for the vertical plane, the tunes are chosen considering the transparency condition number IV.

The choice of a low vertical integer tune also produces much superior performance in terms of DA and EA compared to a higher vertical integer tune.

D. Optimizations with alignment errors

The ring in Fig. 12 (composed of five ARC-Us, three ARC-Ds, and eight long straight sections) has been designed with MAD8 [55] and fully characterized with AT (Accelerator Toolbox) [56] and the ESRF computing cluster [57] to further optimize its performances. Either a ring composed of 72 CELL-Us or a simplified worst case ring with all long SSs replaced by the most chromatic one

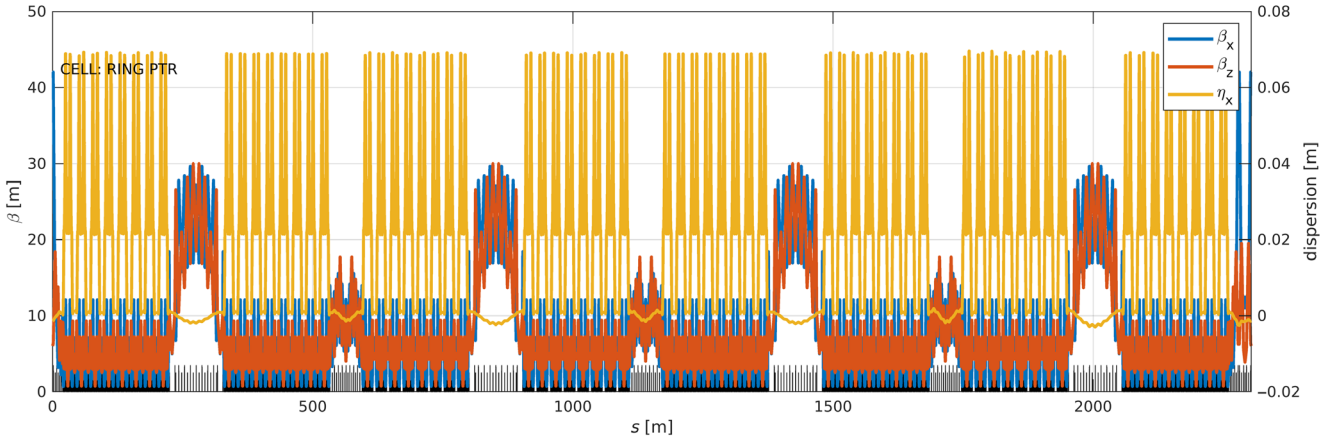

FIG. 12. Possible ring layout including five ARC-Us, three ARC-Ds, three short (56.8 m) SSs, four long (103 m) SSs, and one injection SS.

in Fig. 8 was used for the optimizations. Optimal values for tunes, chromaticities, SD sextupole unbalance ($+\Delta K$ for SD1 and $-\Delta K$ for SD2) are (surprisingly) very similar to the EBS ones [58] ($\Delta K = -5.5$ m^{-3} while for EBS $\Delta K = -1.3$ m^{-3}). The scans are performed averaging over several random alignment error sets each generated with a different starting seed. This avoids misleading conclusions but limits the scans to lower resolution for the same computation time. The values of each point in every scan are averaged over five sets of small alignment errors (drawn from a Gaussian distribution with $\sigma_x = \sigma_y = 1$ μm truncated at 2.5σ) in all quadrupoles and sextupoles; no correction is applied. The horizontal natural emittance values are reported in the scans to emphasize the presence of errors. For DA and EA computation in AT, each test particle is tracked for 2048 turns with 6D motion including rf and radiation damping. Figure 13 displays a chromaticity working point scan. For the H6BA lattice, as for the EBS H7BA, high chromaticity $\xi_{h,v} = (9, 7)$ improves the DA and EA. This is fortunate because large chromaticities are needed to reduce instabilities from collective effects. Again, as for EBS, the tune scan (see Fig. 14) of the H6BA cells is very smooth and shows no evident resonances. This effect is due to the second order cancelation of sextupole aberrations introduced by the "$-\mathcal{I}$" optics [44]. In the case of the H6BA lattice presented in this paper, the variation is really small also due to the extremely small

TABLE III. Comparison of magnet gradients for an H6BA cell with two different vertical integer tunes respecting the transparency condition IV.

Magnet	Units	$Q_v = 78$	$Q_v = 65$
QD0	T/m	−107.5193 (0.17 m)	-
QF1	T/m	110.0 (0.345 m)	110.6 (0.205 m)
QD2	T/m	−92.4 (0.160 m)	−109.2 (0.155 m)
QF3	T/m	91.1 (0.280 m)	91.4 (0.285 m)
QD3	T/m	−91.8 (0.110 m)	−85.7 (0.105 m)
QF4	T/m	90.6 (0.110 m)	86.1 (0.135 m)
QD5	T/m	−93.3 (0.110 m)	−84.6 (0.105 m)
QD6	T/m	−50.3 (0.040 m)	⋯
QF7	T/m	91.3 (0.250 m)	88.9 (0.270 m)
SD1A	T/m^2	−2101 (0.255 m)	−1693 (0.247 m)
SF2A	T/m^2	2041 (0.231 m)	1695 (0.200 m)
SD1B	T/m^2	−1781 (0.255 m)	−1693 (0.111 m)
OF1A	T/m^3	⋯	206809 (0.060 m)
OF1B	T/m^3	−86726 (0.090 m)	⋯
DECF	T/m^4	250173 (thin)	100069 (thin)

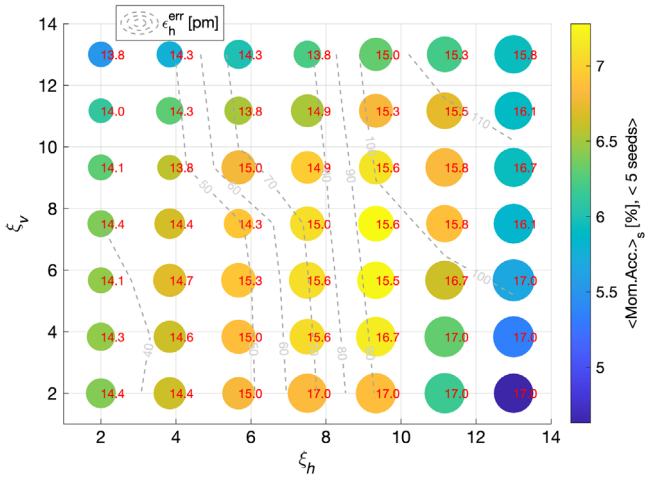

FIG. 13. Chromaticity working point scan. The size of each dot is proportional to the DA (also mentioned in red text in mm). The color is proportional to the average EA along s (*Mom. Acc.* in the figure label). All values are averaged for five seeds of small alignment errors $\sigma_x = \sigma_y = 1$ μm in all quadrupoles and sextupoles (without correction). The tune working point for this scan is fixed to ($Q_h = 134.2$, $Q_v = 73.2$). For DA and EA, 6D tracking with rf and radiation is performed for 2048 turns. The emittance contour lines correspond to the average emittance of lattices without optics correction.

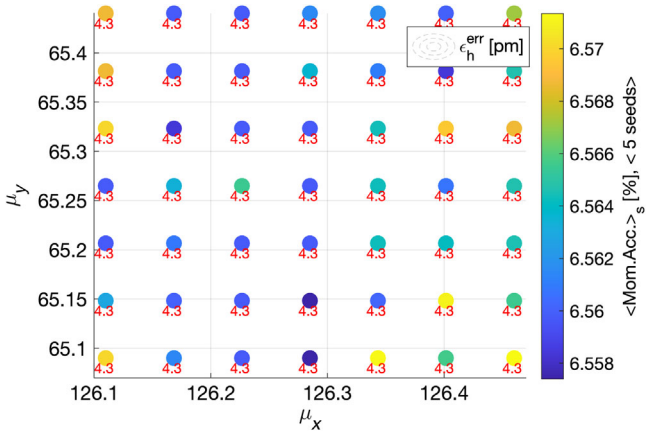

FIG. 14. CELL-U Tune working point scan. The size of each dot is proportional to the DA (also mentioned in red text in mm). The color is proportional to the average EA along s (*Mom. Acc.* in the figure label). All values are averaged for five seeds of small alignment errors $\sigma_x = \sigma_y = 1$ μm in all quadrupoles and sextupoles (without correction). For DA and EA, 6D tracking with rf and radiation is performed for 2048 turns.

variations of the tune with amplitude (see Figs. 10 and 11). Among other optimizations, the optimal values for the defocusing octupole and the focusing decapole are found in the data in Fig. 15.

E. Accelerator performance

Four cases have been studied to outline the performances of the H6BA lattice cell and the impact of straight sections:

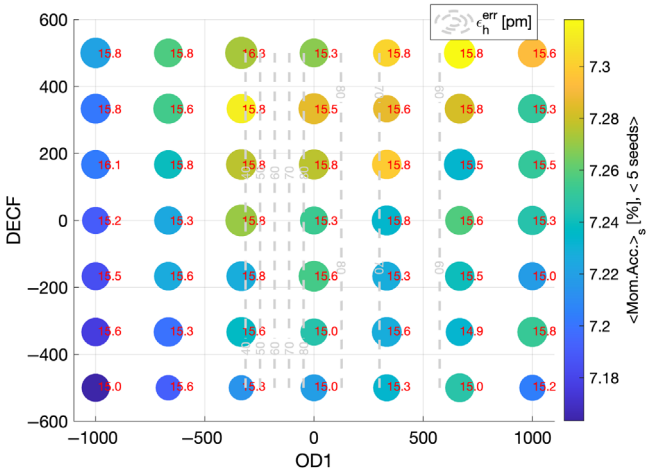

FIG. 15. OD1 and DECF working point scan (variation compared to starting values). The size of each dot is proportional to the DA (also mentioned in red text in mm). The color is proportional to the average EA along s (*Mom. Acc.* in the figure label). The values are averaged for five seeds of small alignment errors $\sigma_x = \sigma_y = 1$ μm in all quadrupoles and sextupoles (without correction). For DA and EA, 6D tracking with rf and radiation is performed for 2048 turns. The emittance contour lines correspond to the average emittance of lattices without optics correction.

(i) a hypothetical *perfect ring* that consists of just the CELL-U and CELL-D

(ii) a *full ring* case including ARC-U, ARC-D, and eight SSs, which delivers an elliptical beam with emittances $\epsilon_{h,v} = (20, 5)$ pm rad

(iii) a *full ring coupled* case including ARC-U, ARC-D, and eight SSs, which delivers a perfect round beam with emittances $\epsilon_{h,v} = (10.6, 10.6)$ pm rad

(iv) a *full ring with errors* including ARC-U, ARC-D, and eight SSs, with small random errors selected from a Gaussian distribution and producing a closed orbit distortion of $\sqrt{<\Delta x^2>} \simeq \sqrt{<\Delta y^2>} \simeq 50$ μm in both planes.

The eight SSs included in the ring are the worst case most chromatic ones in Fig. 8. Optimal sextupole, octupole, and decapole settings determined in the previous Sec. V D are included for all cases.

In general, the coupling control to obtain the *full ring coupled* case may be performed similarly to any other lattice. In the simulations presented here, a random set of skew quadrupoles at every sextupole is scaled in amplitude until full coupling is observed for the ring.

Supposing a septum blade at 15 mm from the beam in the four cases, the DA (see Fig. 16) reaches almost the physical dimension at the septum. DA vs momentum and EA (in Figs. 17 and 18) are also comparable or larger than those of presently operational light sources (see Fig. 1).

Given the moderate variation of tune with amplitude (in Fig. 10), the degradation due to lattice errors is moderate as well. Detailed error and correction analyses will be addressed by further studies and in [49].

Also, comparing the *perfect ring* with the *full ring* cases, it is clear that the SSs have almost no impact

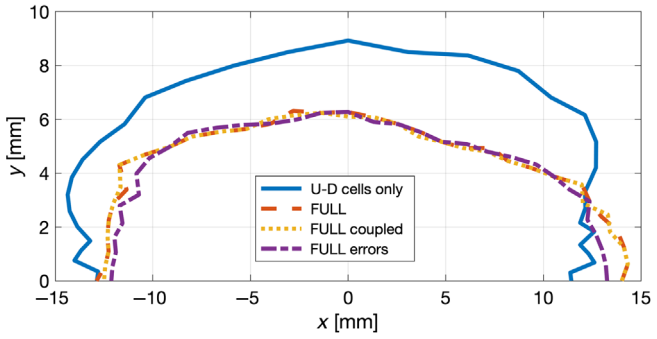

FIG. 16. Dynamic aperture scaled at $\beta_{h,v} = (32.0, 11.8)$ for four cases: the *full ring* layout (including eight SSs), a lattice without long straight sections ("U-D cells only" in legend corresponds to *perfect ring*), a *full ring coupled* layout including SSs and random skew quadrupoles to produce full coupling and a *full ring with errors*. DA limits are determined using 6D tracking simulations of 2048 SR turns with rf and radiation. Tunes and chromaticities for each case are listed in Table IV. Tunes and chromaticities for the case with errors are corrected to the *full ring* case.

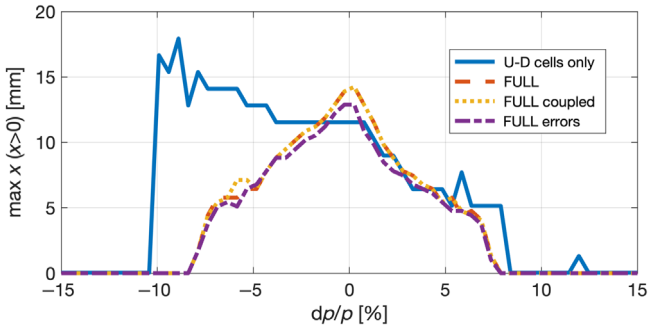

FIG. 17. Maximum horizontal dynamic aperture vs $\delta p/p$ energy deviation scaled at $\beta_{h,v} = (32.0, 11.8)$ m for four cases: the *full ring* layout (including 8 SSs), a lattice without long straight sections ("U-D cells only" in legend corresponds to *perfect ring*), a *full ring coupled* layout including SSs and random skew quadrupoles to produce full coupling and a *full ring with errors*. The limits are determined using 6D tracking simulations of 2048 SR turns with rf and radiation. Tunes and chromaticities for each case are listed in Tab. IV. Tunes and chromaticities for the case with errors are corrected to the *full ring* case.

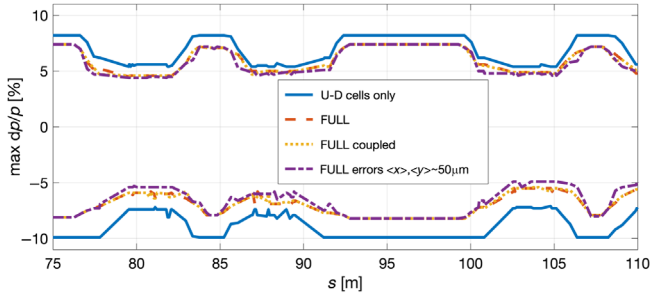

FIG. 18. Energy acceptance for four cases: the *full ring* layout (including eight SSs), a lattice without long straight sections ("U-D cells only" in legend corresponds to *perfect ring*), a *full ring coupled* layout including SSs and random skew quadrupoles to produce full coupling and a *full ring with errors*. The limits are determined using 6D tracking simulations of 2048 SR turns with rf and radiation. The figure concerns the first 35 m of ARC-U in every case. Tunes and chromaticities for each case are listed in Table IV. Tunes and chromaticities for the case with errors are corrected to the *full ring* case.

on the DA (note that the DA is rescaled at the same $\beta_{h,v} = (32, 11.8)$ m for each case). The additional chromaticity introduced by the straight sections is corrected increasing the sextupole strengths in the ARC-U and ARC-D cells. The chromaticity increase from each SS is about 1% in both planes thus about 8% total per plane (for example, for the case of eight SSs in the *full ring* layout). The expected reduction in DA and EA when introducing the SSs is then about 14% [see Eq. (1)] compared to a ring without SSs.

The expected reduction in TL is about 37% [see Eq. (2)] for the *full ring* compared to a ring without SSs.

After optimization, both these limits are actually exceeded as shown in Figs. 17 and 18.

DA at the septum is ~12 mm in all cases studied, with no evident distinction in the horizontal plane when including eight SSs. The EA at septum is about 9.0% (average over one cell is 7.7%) for the ring without straight sections and about 7.3% (average over one cell is 6.6%) for the complete ring (see Figs. 17 and 18). These values are in agreement with the 14% expected reduction due to the increased chromaticity.

The reduction of EA is larger in the presence of small errors, particularly in dispersive regions (e.g., $s = 80$ m in Fig. 18). Overall, it is nevertheless very similar to the EA without errors.

The computed TL for the *full ring* ($\tau^{\text{full}}_{\text{Touschek}} = 237$ h) is comparable to the one of the *perfect ring* ($\tau^{U-D}_{\text{Touschek}} = 239$ h), exceeding the value expected from equation (2) ($\tau^{\text{full,expected}}_{\text{Touschek}} = (1 - 0.37) \times \tau^{U-D}_{\text{Touschek}} = 153$ h) also due to the different bunch length and energy spread (reported in Table IV). A Touschek lifetime of $\tau^{\text{full,errors}}_{\text{Touschek}} = 166$ h is achieved in the presence of errors for typical operational filling mode currents per bunch of 0.1 mA/bunch, $V_{\text{rf}} = 11$ MV and assuming total storage ring impedance of $Z/n = 0.67\ \Omega$. It is noted that the Touschek Lifetime is actually increasing for very low horizontal emittances as shown in [59].

The H6BA TL is larger for all beam modes than the operational TL of existing third generation facilities with similar layout and with emittances 100 times larger.

The frequency map analysis [60] for the *full ring with errors* case is presented in Fig. 19. The same study was done for all cases shown in Figs. 16 and 17.

TABLE IV. Parameters of SR source composed of 72 cells operating at 6 GeV. The vertical emittance is fixed to the value used for lifetime calculation.

	Perfect	Full	Full coupled
C m	1656.5	2456.6	2456.6
ϵ_h pm rad	20.1	20.1	10.6
ϵ_v pm rad	5	5	10.6
Q_h	126.2	134.2	134.2
Q_v	65.2	73.2	73.2
ξ_h	9	9	9
ξ_v	7	7	7
Natural ξ_h	−179	−192	−192
Natural ξ_v	−208	−218	−218
α_c 10^{-5}	4.35	2.93	2.93
δ_E 10^{-4}	7.1	8.2	8.2
$\sigma_z(I_b = 0)$ mm	1.4	2.0	2.0
$\sigma_z(I_b = 0.1$ mA$)$ mm	3.5	5.6	5.6
J_x	1.78	1.29	1.15
U_0 MeV/turn	1.15	3.1	3.1
rf MV	11	11	11
Touschek lifetime h	237	239	273

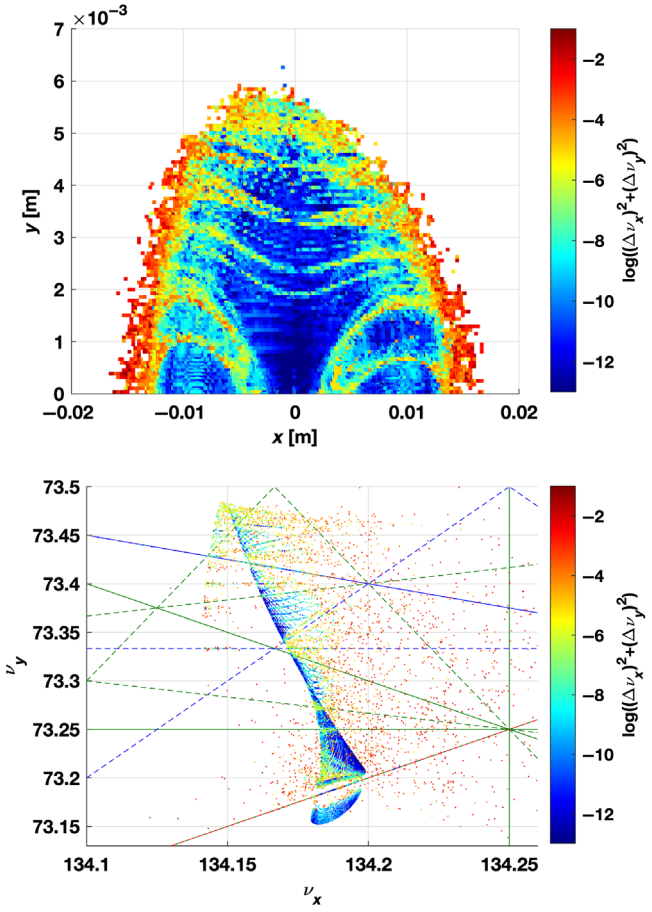

FIG. 19. Frequency map analysis for *full ring with errors*. Configuration space is shown on the top, tune space on the bottom. The diffusion rates are computed based on 6D tracking performed over 2048 turns without radiation.

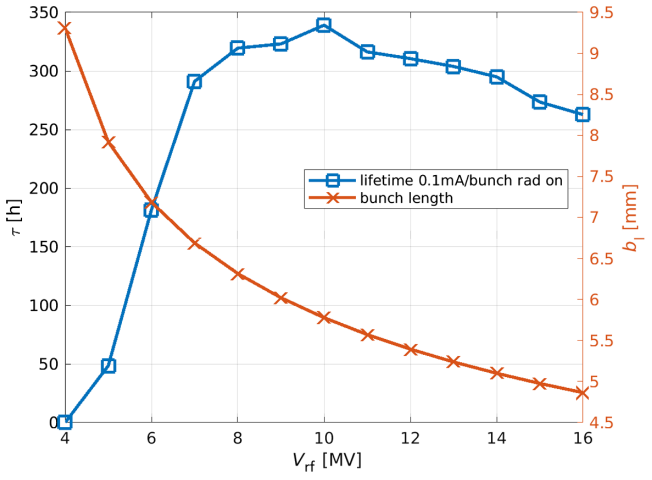

FIG. 20. Bunch length and Touschek lifetime vs rf voltage for a *full ring* lattice.

F. H6BA based large ring table of parameters

A table of relevant parameters of the *full ring* lattice described above is presented in IV.

Looking at the variation of lifetime with rf voltage in Fig. 20, an rf voltage of 11 MV is chosen to take full benefit of the large EA.

The energy loss per turn U_0 is very similar to the EBS one (3.2 MeV for EBS with IDs closed). The same is true for the bunch lengths σ_z. Despite the low $\beta_{h,v}$ at IDs in both planes ($\beta_{x,y}^{\mathrm{ID}} = 2.5$ m), the chromaticities are moderate.

Profiting from the ARC-D sections, the storage ring can operate with constant emittances (regardless of ID gap movements requested by the users) in two modes: elliptic with $\epsilon_{h,v} = (20, 5)$ pm rad or full coupled with $\epsilon_{h,v} = (10.6, 10.6)$ pm rad.

VI. INJECTION CELL DESIGN FOR INJECTED BEAM OSCILLATIONS DEMAGNIFICATION AT IDs

For the lattice presented in these pages, the large β_h at injection (see Figs. 9 and 12) is not needed for efficient injection, but in order to operate with 2.5 mm ID half-gap horizontally and vertically. The demagnification of the injected beam oscillation from the septum ($\beta_h = 42$ m) to the entrance of the undulator ($\beta_h = 5$ m) is about $\times 1/2.9$. This demagnification can be further increased by matching the lattice optics to get even higher β_h at the septum.

Figure 21 shows an injected beam ($\epsilon_h = 10$ nm, $\epsilon_v = 10$ nm, bunch length 3.3 mm, $\sigma_\delta = 0.1\%$) and the stored beam (not to scale) at the two sides of a 2-mm septum blade. The injected beam is as close as possible to the blade to minimize injection oscillations. Three scrapers are placed in the first long SS after injection (at $s \sim 250$ m in Fig. 12) and set to apertures $p = 0.9 \times h_{\mathrm{gap}} \times \sqrt{\frac{\beta_{h,\mathrm{scraper}}}{\beta_{h,\mathrm{ID}}}} \sim 4.5$ mm for $h_{\mathrm{gap}} = 2.5$ mm. The trajectories of the

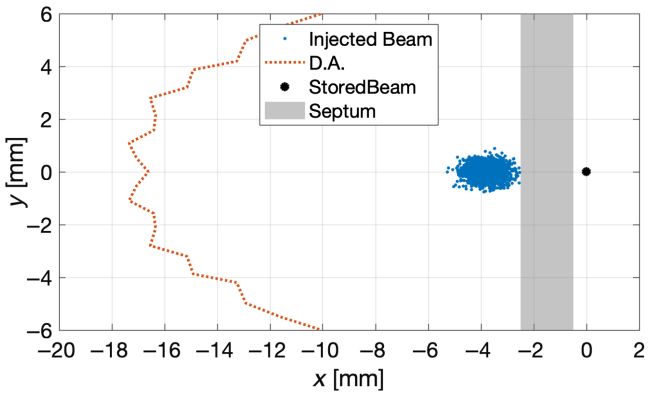

FIG. 21. Injected and stored beam (not to scale) at injection. The beta at injection for this lattice is $\beta_{x,y} = (42.0\ \mathrm{m}, 6.05\ \mathrm{m})$.

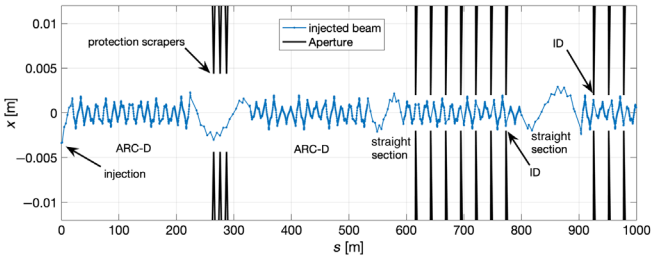

FIG. 22. Trajectory of electrons injected (center of the injected beam) and horizontal apertures. Only the first 1 km is shown for display purposes.

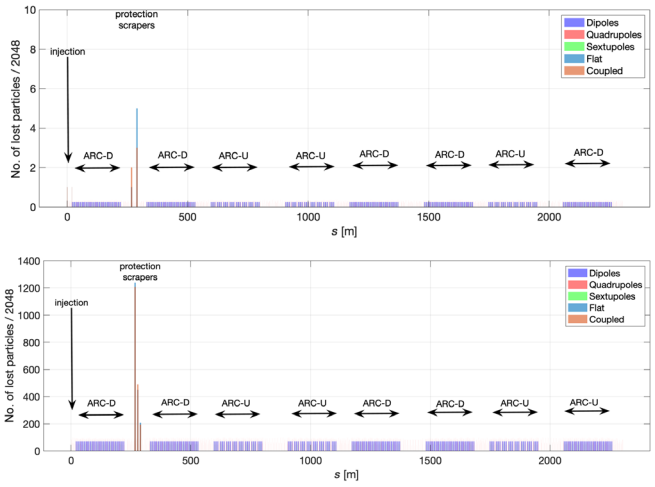

FIG. 23. Location of lost particles during 1000 turns tracking of a 6D beam composed of 2048 e^- injected: at the optimal injection position (top), with a too large horizontal position (bottom). All particles are intercepted by the protection scrapers.

simulated 2048 particles never intercept the 2.5-mm apertures set in the ID straight sections (see Fig. 22).

The few particles lost (5/2048) are all intercepted by the protection scrapers defined in the first long SS (see Fig. 23). In case of injection errors, simulated by a shift of the injected beam position, the protection scrapers intercept all the injected beam protecting the ID magnets. This is true for the *full ring* with or without coupling.

VII. H6BA ENGINEERING

The cell has been designed starting from the EBS H7BA cell (see Fig. 24). All magnets are sized using similar gradients, iron yoke and coils. Only the longitudinal lengths are shorter. All spaces between the elements are assigned for the allocation of extra components such as valves, flanges, bellows, beam position monitors, and steerers assuming the same engineering choices made for EBS. Nevertheless, the x-ray absorbers heat load is about

FIG. 24. EBS cell assembled.

25% less with respect to EBS. Also, the geometry and the space allocation for the crotch chamber and front ends (FE) are as in EBS. There are no components in the critical path for the finalization of the engineering of the H6BA cell.

The H6BA layout is in fact a simplified version of EBS.

All the H6BA components are relaxed copies of the EBS ones. For example, the absorbers have to withstand less heat load, the magnets are smaller and there is less weight on each girder. Fewer components are needed compared to EBS: seven beam position monitors per cell are needed instead of ten used for EBS, thanks to the removal of the central FODO section. The assembly is simpler as well since it excludes the central region of the EBS cell composed of high gradient quadrupoles and combined function dipole-quadrupoles.

A rough estimate of the capital cost for the CELL-U/D is about 70% with respect to the EBS one [6]. The power consumption per CELL is also likely to be about 70% with respect to the EBS one (per unit length of the accelerator).

VIII. H6BA LOW ENERGY SCALING

The H6BA lattice cell design, together with the transparency conditions that allow the introduction of arbitrary straight sections, overcomes the trend to accept smaller DA and EA in order to obtain smaller horizontal equilibrium emittances presently set by synchrotron radiation facility upgrades around the world (see Fig. 1). Thanks to the lattice design presented in this paper, it is possible to achieve small emittances keeping DA largely sufficient for beam accumulation and TL exceeding 10 h for all commonly used operation modes.

The rescaling of optimized solutions for a given layout is very complex. However, it should be noted that the H6BA ring can be scaled with energy (E_0) in a very interesting manner. Rescaling a ring with no wigglers, ϵ_h goes down with E_0^2 and U_0 with E_0^4. Decreasing the energy while keeping the gradients constant would also make such that the ring could become shorter, mainly due to less space required for quadrupoles.

Unfortunately, the (high energy) x-ray flux decreases very fast and finally outweighs the benefits from the increased brilliance due to the smaller ϵ_h.

The example DLS in Fig. 1 is what is obtained by simply scaling H6BA to 4 GeV without lowering the wiggler fields. With this assumption, ϵ_h goes down faster than E_0^2.

The DLS layout example is the ring in Fig. 12 with all the long straight sections included and the rf reallocated in one of the short straight sections of 56.8 m.

The example DLS can deliver at 4 GeV $\epsilon_{h,v} = (2.5, 2.5)$ pm rad round beam with a TL in excess of 100 h.

The recipe for a DLS or any green field high brightness storage ring with large DA and EA is a modular accelerator consisting of basic blocks with well-defined separate functions:

Block 1:	the ARCs, optimized for x-ray delivery, engineering, DA, and EA
Block 2:	Wiggler straight section optimized to achieve the target emittance
Block 3:	rf straight section
Block 4:	Injection straight section optimized for 100% injection efficiency and for injection consistent with undulator gaps fully closed in both planes to 2.5 mm
Block n:	for other needs … .

The modular design relies on the fundamental achievement, which is possible to add to *Block 1*, all the other blocks needed without significantly affecting its DA/EA properties. This is done thanks to the transparency conditions detailed in this paper.

With this modular design, the machine footprint could deviate more from a circle, possibly making it encompass a smaller area.

IX. CONCLUSIONS

The H6BA lattice design for large SR light sources opens a new era for delivering x-ray beams of unprecedented quality for synchrotron radiation based x-ray science.

The potential built into the design is very large and we can just begin to imagine what could be done:

(i) High performance undulators that can have small gaps both in the horizontal and vertical plane

(ii) harmonic cavities could be used to shorten the bunches, rather than lengthening them, thanks to the long beam lifetime

(iii) on-axis, off-phase injection [61], for transparent injection in the SR.

The H6BA lattice in conjunction with a modular design could produce a diffraction limited source with unprecedented characteristics.

The solutions presented are based on the EBS engineering and could be timely realized in line with what was done at ESRF.

With enough cells, even at 3 GeV, the diffraction limit (for x rays of 1 Å wavelength) can be reached in a relatively compact SR (600–700 m) [62].

Based on the present know-how and technology, it is conceivable to build synchrotrons the performance of which are at least 10 times higher than the present state-of-the-art facilities. The long-sought diffraction limit is within our reach. It is possible to push forward the frontier of synchrotron based x-ray science by at least another decade.

[1] R. Chasman, G. K. Green, and E. M. Rowe, Preliminary design of a dedicated synchrotron radiation facility, Technical Report No. BNL–19874, 1974, https://inis.iaea.org/search/search.aspx?orig_q=RN:07223877.

[2] D. Einfeld, J. Schaper, and M. Plesko, Design of a diffraction limited light source (DIFL), in *Proceedings of the Particle Accelerator Conference*, Dallas, TX, 1995 (IEEE, New York, 1995), Vol. 1, pp. 177–179, https://accelconf.web.cern.ch/p95/ARTICLES/TPG/TPG08.PDF.

[3] J. C. Biasci, J. F. Bouteille, N. Carmignani, J. Chavanne, D. Coulon, Y. Dabin, F. Ewald, L. Farvacque, L. Goirand, M. Hahn, J. Jacob, G. LeBec, S. Liuzzo, B. Nash, H. Pedroso-Marques, T. Perron, E. Plouviez, P. Raimondi, J. L. Revol, K. Scheidt, and V. Serrière, A low-emittance lattice for the ESRF, Synchrotron Radiat. News **27**, 8 (2014).

[4] S. C. Leemann, M. Sjöström, and Å. Andersson, First optics and beam dynamics studies on the MAX IV 3 GeV storage ring, Nucl. Instrum. Methods Phys. Res., Sect. A **883**, 33 (2018).

[5] L. Liu, X. R. Resende, A. R. D. Rodrigues, F. H. Sá, and H. Westfahl. Sirius: A 5BA low-emittance lattice with superbends for the New Brazilian Synchrotron Light Source, Synchrotron Radiat. News **26**, 34 (2013).

[6] G. Admans, P. Berkvens, A. Kaprolat, and J.-L. Revol, ESRF Upgrade Programme Phase II (2015–2022): Technical Design Study (2014), https://www.esrf.fr/Apache_files/Upgrade/ESRF-orange-book.pdf.

[7] P. Raimondi, N. Carmignani, L. R. Carver, J. Chavanne, L. Farvacque, G. Le Bec, D. Martin, S. M. Liuzzo, T. Perron, and S. White, Commissioning of the hybrid multibend achromat lattice at the European Synchrotron Radiation Facility, Phys. Rev. Accel. Beams **24**, 110701 (2021).

[8] J. Corbett, X. Huang, M. Lee, P. Lui, and B. Sayyar-Rodsari, Electron beam lifetime in SPEAR3: Measurement and simulation, in *Proceedings of the 22nd Particle Accelerator Conference, PAC-2007, Albuquerque, NM* (IEEE, New York, 2007), pp. 4153–4155, https://accelconf.web.cern.ch/p07/PAPERS/FRPMS064.PDF.

[9] L. Wang, X. Huang, Y. Nosochkov, J. A. Safranek, and M. Borland, Optimization of the dynamic aperture for SPEAR3 Low-emittance Upgrade, in *Proceedings of 3rd International Particle Accelerator Conference, IPAC2012, New Orleans, LA* (JACoW, Geneva, Switzerland, 2012), pp. 1380–1382, https://accelconf.web.cern.ch/ipac2012/papers/tuppc096.pdf.

[10] A. Streun, SLS acceptance and lifetime, in *Proceedings of ESRF workshop nonlinear dynamics in storage rings: From modelling to experiment Grenoble* (2008), http://www.esrf.eu/files/live/sites/www/files/events/conferences/2008/non-linear-beam-dynamics-workshop/pdf/streun_sls.pdf.

[11] P. Brunelle, A. Loulergue, A. Nadji, L. Nadolski, and M.-A. Tordeux, Non linear beam dynamics studies at SOLEIL using experimental frequency map analysis. Conf. Proc. C **100523**, THPE061 (2010), https://accelconf.web.cern.ch/IPAC10/papers/thpe061.pdf.

[12] E. Karantzoulis, C. J. Bocchetta, A. Carniel, M. Ferianis, A. Fabris, F. Iazzourene, R. Nagaoka, M. Svandrlik, L. Tosi, R. P. Walker, and A. Wrulich, Beam lifetime measurements in ELETTRA, in *Proceedings of 5th European Particle Accelerator Conference, EPAC'96, Sitges, Barcelona, Spain* (IOP, Bristol, 1996), https://accelconf.web.cern.ch/e96/PAPERS/WEPG/WEP111G.PDF.

[13] L. Tosi, C. J. Bocchetta, A. Fabris, F. Iazzourene, E. Karantzoulis, R. Nagaoka, M. Svandrlik, P. Walker, and A. Wrulich, Dynamic aperture, comparison of measurements on ELETTRA with simulations, in *Proceedings of the 5th European Particle Accelerator Conference, Sitges, Barcelona, Spain* (IOP, Bristol, 1996), https://accelconf.web.cern.ch/e96/PAPERS/MOPL/MOP086L.PDF.

[14] C. Steier and L. Yang, Touschek lifetime measurements at small horizontal emittance in the ALS, in *Proceedings of the 23rd Particle Accelerator Conference, Vancouver, Canada, 2009* (IEEE, Piscataway, NJ, 2009), pp. 3269–3271, https://accelconf.web.cern.ch/pac2009/papers/th5pfp033.pdf.

[15] W. Decking and D. Robin, Dynamic aperture measurements at the Advanced Light Source, in *Proceedings of the 1999 Particle Accelerator Conference, New York, NY* (IEEE, New York, NY, 1999), pp. 1581–1583, https://accelconf.web.cern.ch/p99/PAPERS/TUP45.PDF.

[16] M. Muñoz, H. L. Owen, and S. L. Smith, Optimisation of the dynamic aperture of DIAMOND, in *Proceedings of the 5th European Particle Accelerator Conference, Sitges, Barcelona, Spain* (IOP, Bristol, 1996), https://accelconf.web.cern.ch/e96/PAPERS/MOPL/MOP043L.PDF.

[17] R. Bartolini and N. G. Wyles, Linear coupling and Touschek lifetime issues at DIAMOND storage ring, in *Proceedings of the 9th European Particle Accelerator Conference, Lucerne, 2004* (EPS-AG, Lucerne, 2004), https://accelconf.web.cern.ch/e04/papers/THPKF071.pdf.

[18] A. Ropert, Dynamic aperture studies at the ESRF, in *Proceedings of the 6th European Particle Accelerator Conference, Stockholm, 1998* (IOP, London, 1998), https://accelconf.web.cern.ch/e98/PAPERS/THP06G.PDF.

[19] B. Nash, F. Ewald, L. Farvacque, J. Jacob, B. Nash, E. Plouviez, J. L. Revol, and K. B. Scheidt. Touschek lifetime and momentum acceptance measurements for ESRF, Conf. Proc. C **110904**, 2923 (2011), https://accelconf.web.cern.ch/ipac2011/papers/thpc008.pdf.

[20] V. Sajaev and L. Emery, Dynamic aperture study and lifetime improvement at the Advanced Photon Source, in *Proceedings of the 21st Particle Accelerator Conference, Knoxville, TN, 2005* (IEEE, Piscataway, NJ, 2005), https://accelconf.web.cern.ch/p05/PAPERS/MPPE064.PDF.

[21] M. Takao, J. Schimizu, Y. Shimosaki, and K. Soutome. Dynamic aperture study at the SPring-8 Storage Ring, in *Proceedings of the International Particle Accelerator Conference, Kyoto, Japan* (ICR, Kyoto, 2010), pp. 4671–4673, https://accelconf.web.cern.ch/IPAC10/papers/thpe067.pdf.

[22] H. Ohkuma, S. Date, K. Fukami, M. Masaki, T. Nakamura, T. Ohshima, K. Soutome, S. Takano, K. Tamura, K. Takao, H. Tanaka, and N. Kumagai, Operation and performance of the SPring-8 Storage Ring, in *Proceedings of the 18th Particle Accelerator Conference, New York, 1999* (IEEE, New York, 1999), https://accelconf.web.cern.ch/p99/PAPERS/WEP35.PDF.

[23] R. Bacher *et al.*, PETRA III—status of the storage ring, AIP Conf. Proc. **879**, 175 (2007).

[24] X. Gavaldà, J. Keil, G. Sahoo, and R. Wanzenberg, PETRA III storage ring performance improvement based on multi-objective genetic algorithms (MOGA), in *Proceedings of 9th International Particle Accelerator Conference, IPAC'18, Vancouver, BC, Canada* (JACoW, Geneva, Switzerland, 2018), https://accelconf.web.cern.ch/ipac2018/papers/thpaf030.pdf.

[25] H. Tarawneh, M. Eriksson, L.-J. Lindgren, and B. Anderberg, MAX-IV lattice, dynamic properties and magnet system, Nucl. Instrum. Methods Phys. Res., Sect. A **508**, 480 (2003).

[26] E. Karantzoulis, ELETTRA 2.0—the diffraction limited successor of ELETTRA, Nucl. Instrum. Methods Phys. Res., Sect. A **880**, 158 (2018).

[27] E. Karantzoulis, The diffraction limited light source ELETTRA 2.0, in *Proceedings of 8th International Particle Accelerator Conference, Copenhagen, Denmark* (JACoW, Geneva, Switzerland, 2017), pp. 2660–2662, https://inspirehep.net/files/9c06132d36c35ce1991211cdffa438a3.

[28] F. H. de Sá, L. Liu, and X. R. Resende, Optimization of nonlinear dynamics for Sirius, in *Proceedings of the 7th International Particle Accelerator Conference, Busan, Korea* (JACoW, Geneva, Switzerland, 2016), pp. 3409–3412, https://accelconf.web.cern.ch/ipac2016/papers/thpmr012.pdf.

[29] A. Streun, T. Garvey, L. Rivkin, V. Schlott, T. Schmidt, P. Willmott, and A. Wrulich, SLS-2 the upgrade of the Swiss Light Source, J. Synchrotron Radiat. **25**, 631 (2018).

[30] Christoph Steier, A. Madur, B. Bailey, K. Berg, A. Biocca, A. Black, P. Casey, D. Colomb, B. Gunion, N. Li, Sharon Marks, H. Nishimura, C. Pappas, K. Petermann, G. Portmann, Soren Prestemon, A. Rawlins, D. Robin, S. Rossi, and J. Wu, Completion of the brightness upgrade of the ALS, J. Phys. Conf. Ser. **493**, 012030 (2014).

[31] R. Bartolini *et al.*, Double-double bend achromat cell upgrade at the Diamond Light Source: From design to commissioning, Phys. Rev. Accel. Beams **21**, 050701 (2018).

[32] H. Tanaka, Current status of the SPring-8 Upgrade Project, Synchrotron Radiat. News **27**, 11 (2014).

[33] A. Loulergue, P. Alexandre, P. Brunelle, L. Hoummi, O. Marcouillé, A. Nadji, L. Nadolski, R. Nagaoka, K. Tavakoli, M.-A. Tordeux, and A. Vivoli, Baseline lattice for the upgrade of SOLEIL, in *Proceedings of 9th International Particle Accelerator Conference, IPAC'18, Vancouver, BC, Canada* (JACoW, Geneva, Switzerland, 2018), page THPML034, 10.18429/JACoW-IPAC2018-THPML034.

[34] Y. Jiao, G. Xu, X.-H. Cui, Z. Duan, Y.-Y. Guo, P. He, D.-H. Ji, J.-Y. Li, X.-Y. Li, C. Meng, Y.-M. Peng, S.-K. Tian, J.-Q. Wang, N. Wang, Y.-Y. Wei, H.-S. Xu, F. Yan, C.-H. Yu,

Y.-L. Zhao, and Q. Qin, The HEPS project, J. Synchrotron Radiat. **25**, 1611 (2018).

[35] T. E. Fornek. Advanced Photon Source Upgrade Project preliminary design report, Report No. APSU-2.01-RPT-003, 2017, https://publications.anl.gov/anlpubs/2019/07/153666.pdf.

[36] C. G. Schroer, I. Agapov, W. Brefeld, R. Brinkmann, Y.-C. Chae, H.-C. Chao, M. Eriksson, J. Keil, X. Nuel Gavaldà, R. Röhlsberger, O. H. Seeck, M. Sprung, M. Tischer, R. Wanzenberg, and E. Weckert, PETRA IV: The ultralow-emittance source project at DESY, J. Synchrotron Radiat. **25**, 1277 (2018).

[37] H. Onuki and P. Elleaume, *Undulators, Wigglers and Their Applications*, (Taylor & Francis, London, 2002).

[38] C. Sun, D. Robin, H. Nishimura, Christoph Steier, and Weishi Wan, Small-emittance and low-beta lattice designs and optimizations, Phys. Rev. Accel. Beams **15**, 054001 (2012).

[39] Y. Cho. Optimization of {beta} functions through insertion devices (1985), https://www.osti.gov/biblio/376364.

[40] N. Carmignani. *Touschek Lifetime Studies and Optimization of the European Synchrotron Radiation Facility: Present and Upgrade Lattice* (Springer, New York, 2015).

[41] R. Versteegen, P. Berkvens, N. Carmignani, L. Farvacque, S. Liuzzo, B. Nash, T. Perron, P. Raimondi, and S. White, Collimation scheme for the ESRF upgrade, in *Proceedings of the 6th International Particle Accelerator Conference, IPAC-2015, Richmond, VA, 2015* (JACoW, Geneva, Switzerland, 2015), page TUPWA017, https://accelconf.web.cern.ch/ipac2015/papers/tupwa017.pdf.

[42] C. Benabderrahmane, J.-C. Biasci, J.-F. Bouteille, J. Chavanne, L. Farvacque, L. Goirand, G. Le Bec, S. Liuzzo, P. Raimondi, and F. Villar, Magnets for the ESRF-EBS Project, in *Proceedings of the 7th International Particle Accelerator Conference, IPAC-2016, Busan, Korea* (JACoW, Geneva, Switzerland, 2016), page TUPMB001, https://accelconf.web.cern.ch/ipac2016/papers/tupmb001.pdf.

[43] J. Bengtsson and A. Streun. Robust design strategy for SLS-2, Paul Scherrer Institute Technical Report No. SLS2-BJ84-001-2, 2017.

[44] H. Wiedemann, *Particle Accelerator Physics*, 3rd ed. (Springer, Berlin, 2007).

[45] M. Borland. Simulation of swap-out reliability for the Advance Photon Source Upgrade (2017), https://accelconf.web.cern.ch/napac2016/papers/wepob02.pdf.

[46] Z. Duan, J. Chen, Y. Guo, D. Ji, Y. Jiao, C. Meng, Y. Peng, and G. Xu. Simulation of injection efficiency for the High Energy Photon Source, in *Proceedings of the 10th International Particle Accelerator Conference, IPAC-2019, Melbourne, Australia, 2019* (JACoW, Geneva, Switzerland, 2019), page TUPGW048, https://accelconf.web.cern.ch/ipac2019/papers/tupgw048.pdf.

[47] S. Papadopoulou, F. Antoniou, and Y. Papaphilippou, Emittance reduction with variable bending magnet strengths: Analytical optics considerations and application to the Compact Linear Collider damping ring design. Phys. Rev. Accel. Beams **22**, 091601 (2019).

[48] R. Nagaoka and A. Wrulich, Emittance minimisation with longitudinal dipole field variation, Nucl. Instrum. Methods Phys. Res., Sect. A **575**, 292 (2007).

[49] I. Agapov, S. A. Antipov, R. Bartolini, R. Brinkmann, Y.-C. Chae, D. Einfeld, T. Hellert, M. Hüning, M. A. Jebramicik, J. Keil, C. Li, R. Wanzenberg, P. Raimondi, and S. Liuzzo, The PETRA IV storage ring design based on multi-bend achromat optics, Phys. Rev. ST Accel. Beams (to be published).

[50] Y. Cai, K. Bane, K. Bertsche, A. Chao, R. Hettel, X. Huang, Z. Huang, C. Ng, Y. Nosochkov, A. Novokhatski, T. Rabedeau, J. Safranek, G. Stupakov, L. Wang, M.-H. Wang, and L. Xiao, A baseline design for PEP-X: An ultra-low emittance storage ring, Conf. Proc. C, **100523**: WEPEA074, 2010, https://accelconf.web.cern.ch/IPAC10/papers/wepea074.pdf.

[51] M.-H. Wang, Y. Nosochkov, K. Bane, Y. Cai, R. Hettel, and X. Huang, Lattice design and optimization for the PEP-X ultra low emittance storage ring at SLAC, Nucl. Instrum. Methods Phys. Res., Sect. A **649**, 30 (2011).

[52] S. White, J. Chavanne, M. Dubrulle, G. Le Bec, E. Plouviez, P. Raimondi, and B. Roche, Damping of injection perturbations at the European Synchrotron Radiation Facility, Phys. Rev. Accel. Beams **22**, 032803 (2019).

[53] M. Hara, T. Nakamura, T. Takada, and H. Tanaka, Use of long straight sections of SPring-8, Rev. Sci. Instrum. **63**, 355 (1992).

[54] B. W. Montague, Linear optics for improved chromaticity correction, Report No. LEP-Note-165, 1979.

[55] F. C. Iselin, MAD8 Physics guide, https://cern.ch/mad8/doc/phys_guide.pdf, 1992 [Online; accessed February 11, 2022].

[56] B. Nash, N. Carmignani, L. Farvacque, S. Liuzzo, T. Perron, P. Raimondi, R. Versteegen, and S. White, New functionality for beam dynamics in Accelerator Toolbox (AT), in *Proceedings of the 6th International Particle Accelerator Conference, IPAC-2015, Richmond, VA, 2015* (JACoW, Geneva, Switzerland, 2015), page MOPWA014, https://accelconf.web.cern.ch/ipac2015/papers/mopwa014.pdf.

[57] G. Foerstner. ESRF computing cluster (private communication).

[58] N. Carmignani, L. Farvacque, S. Liuzzo, B. Nash, T. Perron, P. Raimondi, R. Versteegen, and S. White, Linear and nonlinear optimizations for the ESRF Upgrade Lattice, in *Proceedings of the 6th International Particle Accelerator Conference, IPAC-2015, Richmond, VA, 2015* (JACoW, Geneva, Switzerland, 2015), page TUPWA013, https://accelconf.web.cern.ch/ipac2015/papers/tupwa013.pdf.

[59] MAX IV detailed design report (2010), https://www.maxiv.lu.se/wp-content/plugins/sharepoint-plugin/ajax/downloadFile.php?site_id=MAXIV&version_series_id=38&repository_id=0fbdb5b5-c377-4ff8-9350-6889fdf4c076.

[60] J. Laskar, Introduction to frequency map analysis, in *Hamiltonian Systems with Three or More Degrees of*

Freedom, edited by Carles Simó (Springer, Dordrecht, Netherlands, 1999), pp. 134–150.

[61] M. Aiba, B. Goddard, K. Oide, Y. Papaphilippou, Á. Saá Hernández, D. Shwartz, S. White, and F. Zimmermann, Top-up injection schemes for future circular lepton collider, Nucl. Instrum. Methods Phys. Res., Sect. A **880**, 98 (2018).

[62] J. Kim, X. Huang, P. Raimondi, J. Safranek, M. Song, and K. Tian, A hybrid multi-bend achromat lattice design for SSRL-X, in *Proceedings of the 13th International Particle Accelerator Conference, IPAC-2022, Bangkok, Thailand* (JACoW, Geneva, Switzerland, 2022), page MOPOST054, 10.18429/JACoW-IPAC2022-MOPOST054.